# Simultaneous measurement of temperature and liquid refractive index based on fiber open Fabry-Pérot cavity and Bragg grating*

**LIU Qinpeng**, WANG Danyang, LI Xingrui, GAO Hong, and YU Dakuang**
*College of Science, Xi'an Shiyou University, Xi'an 710065, China*

(Received 11 November 2023; Revised 3 April 2024)


A temperature and refractive index sensor based on fiber Bragg grating (FBG) end surface cascade open Fabry-Pérot (FP) cavity has been designed and demonstrated experimentally. The open FP cavity has been fabricated on the end face of an FBG by dislocation fusion in this work, the open FP cavity could be used for refractive index sensing, and the temperature is measured by the FBG. The working principle of the sensor and the method of improving the sensitivity are analyzed by theoretical simulation. The refractive index sensitivity of the sensor is 1 108.4 nm/RIU, while the maximum fluctuation of the sensor stability experiment detection is 0.005 nm. The results show that it has satisfactory characteristics. The sensor is a compact all-fiber structure, so it has potential applications in the field of temperature refractive index sensing, such as biomedical and capacitor electrolyte detection.

**Document code:** A **Article ID:** 1673-1905(2024)08-0477-6
**DOI** https://doi.org/10.1007/s11801-024-3249-4

The refractive index detection and temperature in biomedicine, engineering applications, and battery dete ction has important potential applications[1-5]. Especially in electrochemical detection, the redox reaction occurs when the electrolyte works, which causes small changes of temperature and refractive index. Optic fiber sensors have the advantages of corrosion resistance, small structure size, high temperature resistance and so on. Therefore, various optic fiber refractive index and temperature sensor structures have been designed and produced in recent years, such as localized surface plasmon resonance (LSPR), Mach-Zehnder interferometer (MZI), tilted fiber Bragg grating (TFBG) and Fabry-Pérot (FP)[5-10]. Among them, the fiber optic FP sensor structure design is compact and flexible, which has attracted many researchers' interest. The advantage of the open FP cavity structure is that the measured object could directly enter the cavity for sensing, so this sensing method is more accurate and real-time. The structures of the open FP cavity has been extensive researched, and different fabrication methods have been proposed as follows. In the first type, the open capillary glass tube is used as the cavity, such as the polished glass tube showing a C-type structure[11-14]. For example, WU et al[11] fused a short C-type fiber between two single-mode fibers to create an FP cavity structure. The C-type structure is asymmetry, no convection could be formed, and there might be liquid residue in the cavity during sensing. In addition, other structure was that two optic fibers were glued to both ends of the microporous glass tube, but its sensing performance and temperature resistance range are limited by the glue performance[15]. Secondly, intrinsic corrosion on optic fiber, femtosecond laser or excimer laser have been used to punch hole on the fiber to form an open cavity, and other ways are that hydrofluoric acid to etch the fiber[16-19]. TIAN et al[16] used a femtosecond laser to punch air holes in the fiber to form air cavity, and the refractive index sensitivity and temperature sensitivity were 867.76 nm/RIU and 7.8 pm/°C, respectively. The methods are simple to form cavity, but high cost, and the smooth degree of FP cavity end face is greatly affected by the instrument and operation, so the contrast and reflected light intensity of the spectrum are limited. Thirdly, the dislocation fusion method is used to fuse a segment of optic fiber in the middle of two single mode fibers (SMFs) to form an open FP cavity. NI et al[20] fused a thin fiber in the middle of two SMFs to form an open FP cavity. The FP structure formed is completely open, which is good structural robustness[19-21].

* This work has been supported in part by the National Natural Science Foundation of China (Nos.61735014 and 61927812), the Shaanxi Provincial Education Department (No.18JS093), the Natural Science Basic Research Program of Shaanxi Province (No.2024JC-YBMS_530), the Operation Fund of Logging Key Laboratory of Group Company (No.2021DQ0107-11), and the Graduate Student Innovation Fund of Xi'an Shiyou University (Nos.YCS23213178 and YCS22213185).
** LIU Qinpeng is an associate professor at the School of Science, Xi'an Shiyou University. He received his Ph.D. degree in Optical Engineering from Northwestern Polytechnical University in 2015. His current research interests include optical fiber sensing and their applications. E-mail: lqp1977@163.com

The temperature changes are intertwined with refractive index interaction, so temperature measurement is necessity when detect refractive index. Even through the sensor has low cross temperature interference, it has a certain impact on the measurement accuracy. The fiber Bragg grating (FBG) could detect temperature without being affected by refractive index. Aiming at the problem of temperature interference when the open FP cavity sensor refractive index sensing, the FP cavity has been formed by dislocation at the end of FBG on the premise of ensuring the compactness in this work. The sensor is simple and low cost to manufacture, and operable only required fusion and cut, which has a potential application prospect for capacitor electrolytes.

In the measurement of external ambient biochemical refractive index, direct contact is more accurate and real-time, the open FP cavity refractive index sensor is small size and flexible design in the optic fiber sensor, so we choose the open FP cavity to detect the refractive index. At the same time, the liquid refractive index is disturbed by the change of ambient temperature, so temperature differentiation detection is also necessary. Therefore, under this background demand, we propose to fuse an open FP cavity at the back of the FBG, and a segment of SMF is fused in the middle through dislocation fusion to act as a bond.

The schematic diagram of the optic fiber open FP cavity sensor is shown in Fig.1. Assume $R_1$ and $R_2$ are reflection rates of optic fiber end face respectively. The refractive indices of air and SMF are $n_{\mathrm{AIR}}$ and $n_{\mathrm{SMF}}$. The formula of $R_1$ is expressed as

$$R_1 = R_2 = \left(\frac{n_{\mathrm{SMF}} - n_{\mathrm{AIR}}}{n_{\mathrm{SMF}} + n_{\mathrm{AIR}}}\right)^2 = R. \tag{1}$$

When half wave loss is ignored, the phase $\Delta\varphi$ of light from $R_1$ to $R_2$ is

$$\Delta\varphi = \frac{4\pi nL}{\lambda_m} = (2m+1)\pi, \quad \lambda_m = \frac{4nL}{(2m+1)}, \tag{2}$$

where $n$ is refractive index of the FP cavity medium, and $\lambda_m$ is the valley wavelength of order $m$. The free spectral range (*FSR*) can be expressed as the distance between two valley wavelengths, and its formula can be expressed as

$$FSR = \lambda_{m+1} - \lambda_m = \frac{\lambda_{m+1}\lambda_m}{2nL}. \tag{3}$$

Since $R_1$ and $R_2$ are equal in data in this structure, the expression of reflected light intensity is

$$I_R = \frac{4R\sin^2\left(\Delta\varphi/2\right)}{(1+R)^2 + 4R\sin^2\left(\Delta\varphi/2\right)} I_0. \tag{4}$$

It can be seen from Eqs.(2) and (3) that the phase $\Delta\varphi$ changes with the refractive index in the cavity, which affects the change of reflected light. Therefore, detecting the reflected light under different refractive indices can achieve the refractive index sensing. The simulation of light wavelength shift under different refractive indices is shown in Fig.2(a). It can be seen that the wavelength of reflected light regularly red shifts with the increase of refractive index.

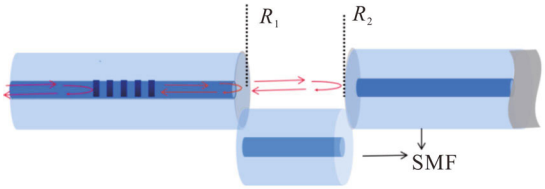


**Fig.1 Schematic diagram of optic fiber FP cavity sensor**

Combined with Eq.(2), the refractive index sensitivity of the sensor is[20]

$$S_{\mathrm{FP},n} = \frac{\mathrm{d}\lambda_m}{\mathrm{d}n} = \frac{4L}{2m+1}. \tag{5}$$

As can be seen from Eqs.(2) and (5), when the cavity length and order are fixed, the refractive index sensitivity of the fixed order can be calculated by tracking the red shift of the corresponding wavelength of the refractive index in a certain range. Combined with Eq.(5), the refractive index sensitivity of different cavity lengths of the same order is calculated, as shown in Fig.2(b). It can be concluded that the refractive index sensitivity of the identical order is positively correlated with the cavity length. When the cavity length increases, the *FSR* of the spectrum decreases, and the corresponding wavelength of the identical order decreases. Therefore, when the corresponding wavelength of an identical order is selected for refractive index sensing, the sensitivity of the sensor can be increased by making a longer cavity length, and the specific method is to find the corresponding wavelength of the same order. When the order is similar, the sensitivity difference is not significant.

According to the *FSR* simulation based on Eq.(3), as shown in Fig.2(b), the increase of cavity length leads to decrease of *FSR*, increasing sensitivity requires cavity length to be increased as much as possible, so we need to combine the actual demand in the selection of cavity length range, to achieve a balance between the sensitivity and the *FSR*. The refractive index in the cavity is 1.342 RIU and the order $m$ is 146, the sensitivity is 1.092 2—1.365 2 μm/RIU when the cavity length is 80—100 μm according to the simulation results.

The temperature sensitivity of the all-fiber FP cavity sensor is[22]

$$S_{\mathrm{FP},T} = \frac{\mathrm{d}\lambda_m}{\mathrm{d}T} = \left(\beta_{\mathrm{FP}} + \alpha_{\mathrm{FP}}\right)\lambda_m, \tag{6}$$

where $\beta$ and $\alpha$ are thermo-optical coefficient and thermal expansion coefficient, respectively. Considering the temperature interference, the FBG is cascaded to measure the temperature of the open FP cavity, and the temperature sensitivity of the FBG is[23]

$$S_{\mathrm{FP},T} = \frac{\mathrm{d}\lambda_m}{\mathrm{d}T} = \left(\beta_{\mathrm{FP}} + \alpha_{\mathrm{FP}}\right)\lambda_m. \tag{7}$$

The formula can be obtained by setting the sensitivity of FP and FBG as the temperature refractive index sensing matrix[23], and the expression is as follows

$$\begin{bmatrix}\Delta n\\ \Delta T\end{bmatrix}=\begin{bmatrix}S_{\mathrm{FP},n} & S_{\mathrm{FP},T}\\ S_{\mathrm{FBG},n} & S_{\mathrm{FBGP},T}\end{bmatrix}\begin{bmatrix}\lambda_{\mathrm{FP}}\\ \lambda_{\mathrm{FBG}}\end{bmatrix}, \tag{8}$$

where $S_{\mathrm{FP},n}$ and $S_{\mathrm{FBG},n}$ are the refractive index sensitivities of FP cavity and FBG, respectively, and $S_{\mathrm{FP},T}$ and $S_{\mathrm{FBG},T}$ are the temperature sensitivities of FP cavity and FBG, respectively. On the base of Eq.(8), the temperature and refractive index detection of the sensor can be calculated separately, so that the refractive index or temperature parameter can be measured according to the measurement requirements.

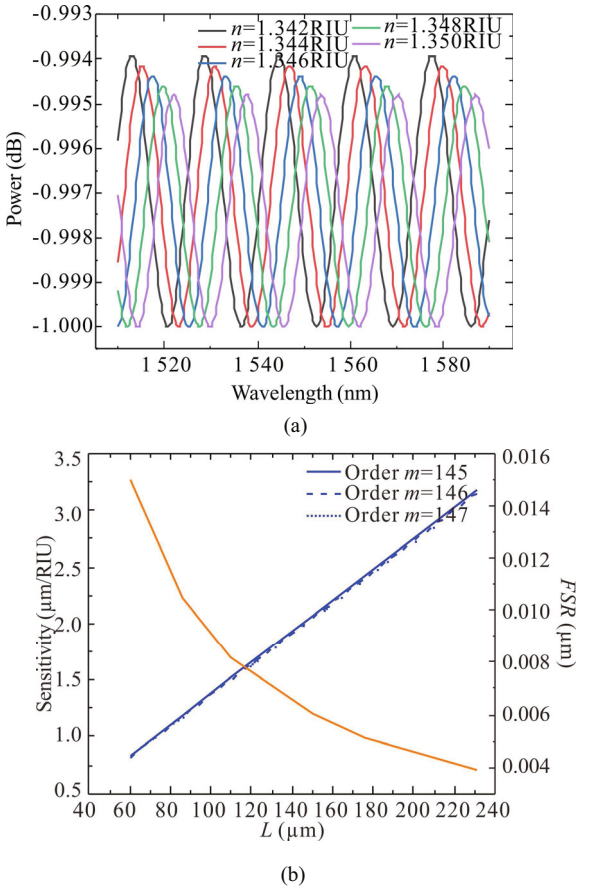


**Fig.2 (a) Simulation of refractive index sensing in FP cavity; (b) Simulation of sensitivity and *FSR* versus cavity length**

Fabrication of sensor through on the end face of the FBG fused an open FP cavity. The open FP cavity structure is compact in tens of microns, so the overall volume of the sensor is small. Meanwhile, only fusion is used to ensure the robustness of the sensor structure.

Sensor production is mainly divided into three steps as follows. First of all, a standard FBG was taken and cleaned, and its end face was cut flat with a cutter. And then use the fusion machine (S177B) to adjust the displacement of SMF (SMF128) end face in the horizontal and vertical directions, so that the SMF cladding was at least 10 μm at the lower end of the fiber core with FBG, adjust the fusion program, and fuse the end face. The dislocation fusion diagram above is shown in Fig.3. It should be noted that in order to ensure the dislocation fusion with flat end faces, the fusion point should be placed on the right side of the arc discharge of the fusion machine to offset 20 μm, and the discharge intensity should be reduced to 45 dB, the advanced distance reduced to 25 μm, and the discharge time should be 200 ms. Secondly, a cavity of micron scale was cut out. Sensitivity and *FSR* are mutually restricted when the open cavity length increases, and the cavity length is cut off according to our requirements. We fixed the misplaced optic fiber on the cutter, and then placed the fiber under the microscope, and moved the misplaced point slightly under the microscope, the cavity length was cut until we needed, as shown in Fig.3(c). Thirdly, fix the cut optic fiber at the left end of the fusion machine, place a single-mode optic fiber at the right end, adjust the optic fiber core alignment between the SMF on the right and FBG on the left, and fuse it to form the FP cavity. The finished structure diagram is shown in Fig.3(e), and its cavity length is 85.8 μm. It can be seen from the above that the sensor is simple to manufacture, with low cost and small size.

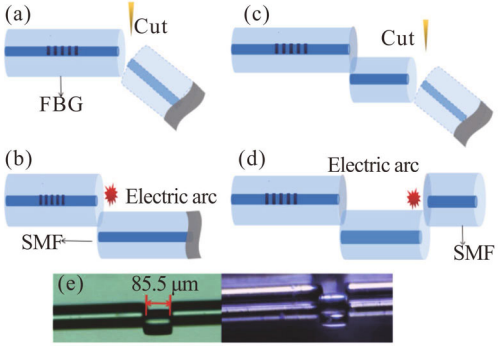


**Fig.3 (a)—(d) Sensor fabrication process; (e) Picture of sensor under microscope**

In order to study the sensor's refractive index and temperature sensing performance, we constructed a refractive index and temperature sensing system respectively, as shown in Fig.4. The demodulation device of the sensor is the optical sensing interrogator (TV125), which has a wavelength range of 1 510—1 590 nm, the wavelength resolution of 0.001 nm, and the wavelength sampling interval of 0.005 nm. The reflected light signal of the sensor was recorded on the computer through the demodulation. In electrochemical detection, some electrolytes are chosen to use inorganic salts, such as LiCl[4,5,24]. The NaCl has similar chemical properties, so it is selected as the refractive index detection quantity. For refractive index sensing system, the solution of 6%—10% NaCl was prepared with deionized water in the beaker, and the refractive index of the solution was standardized with Abbe refractoscope, ranging from

1.343 RIU to 1.351 RIU. The sensor was placed in a beaker with different refractive index liquids for refractive index sensing. The temperature controller (YM-CDC-R80) has a temperature resolution of 0.01 ℃. The sensor was put into temperature controller to simulate the sensing at different temperatures.

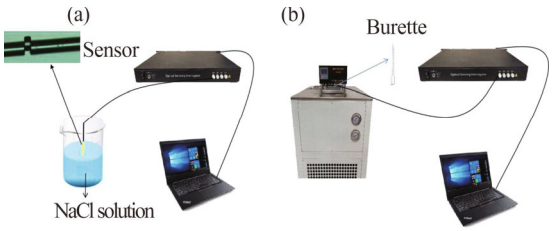


**Fig.4 (a) Schematic diagram of refractive index sensing experimental system; (b) Schematic diagram of temperature sensing experimental system**

In the refractive index sensing experiment at constant temperature, we first used deionized water to configure NaCl solution with a concentration from 6% to 10%, changed by 1% each time, and then used Abbe refractometer to calibrate the refractive index. The optic fiber sensor was completely placed in a beaker with a refractive index of 1.343 5 RIU for 5 min, and the spectra were recorded in five groups with a computer, and then the sensor was taken out, rinsed with deionized water, and then dried naturally. Repeat the above steps to detect the sensor in each solution with different refractive indices, and record them. The spectra detected for refractive index sensing are shown in Fig.5(a). With the increase of refractive index, the wavelength was red shifted. The standard deviation of the five groups of data obtained from each refractive index point was calculated, and then the linear fitting diagram of the refractive index sensor with error rod is shown in Fig.5(b). It can be obtained that the sensitivity of the sensor's refractive index sensing is 1 108.413 5 nm/RIU, and the fit degree is 0.997. The length of the FP cavity is 85.8 μm, and the theoretical refractive index sensitivity is 1 171.3 nm/RIU according to the simulation, so that the experimental results are the same as the theoretical values. FBG in the core was protected by cladding and was not affected by refractive index.

The temperature sensing spectra of the sensor are shown in Fig.6. In order to protect the sensor structure during the temperature detection process, the refractive index of 1.346 9 RIU resolution was filled in a dropper, and then the sensor was placed in the dropper for packaging. During the temperature tested, put the dropper into the temperature controller for water bath heating. When the temperature rises from 4 ℃ to 24 ℃, changed by 4 ℃ every time, stayed at each temperature point for 5 min and recorded 5 points. Five sets of data for each temperature point were taken to get the average and calculate standard deviation, and the two groups of temperature points with error bars were fitted together. The FP and FBG fitting data diagrams are shown in Fig.7(a) and (b), respectively, and its temperature sensitivity is −0.103 9 nm/℃ and 0.010 1 nm/℃, the fit degree is 0.985 and 0.998. The refractive index effect of NaCl solution was not significant when the temperature changed little.

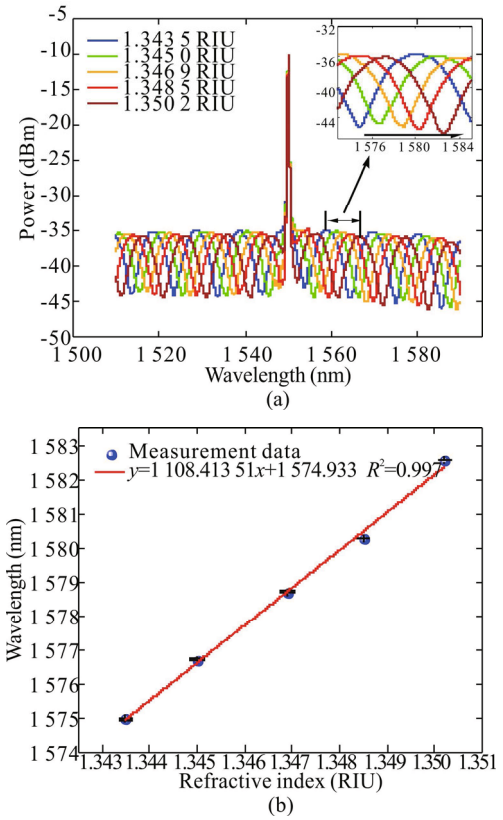


**Fig.5 (a) Spectral diagram of refractive index sensing; (b) Linear fitting diagram of refractive index sensing**

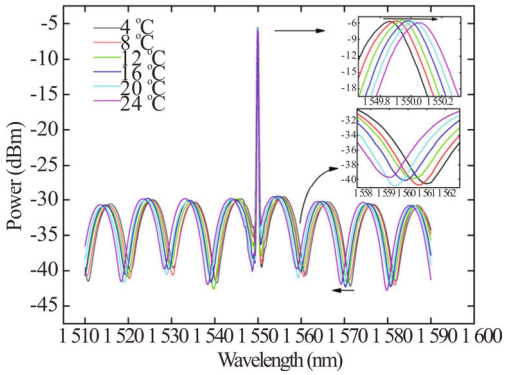


**Fig.6 Temperature sensing spectra of the sensor**

The FBG cladding is silica material, it is not subject to NaCl corrosion or reaction, so FBG protected by cladding is only used for temperature detection. When measuring refractive index, the wavelength shift of the sensor FP cavity was affected by both refractive index and temperature changes. The refractive index and temperature sensitivity of the sensor was obtained by establishing the cross matrix, and bring the sensitivity parameter into Eq.(8) to get

$$\begin{bmatrix}\Delta n\\ \Delta T\end{bmatrix}=\begin{bmatrix}1108.413\,5 & -0.103\,9\\ 0 & 0.010\,1\end{bmatrix}\begin{bmatrix}\lambda_{FP}\\ \lambda_{FBG}\end{bmatrix}. \tag{9}$$

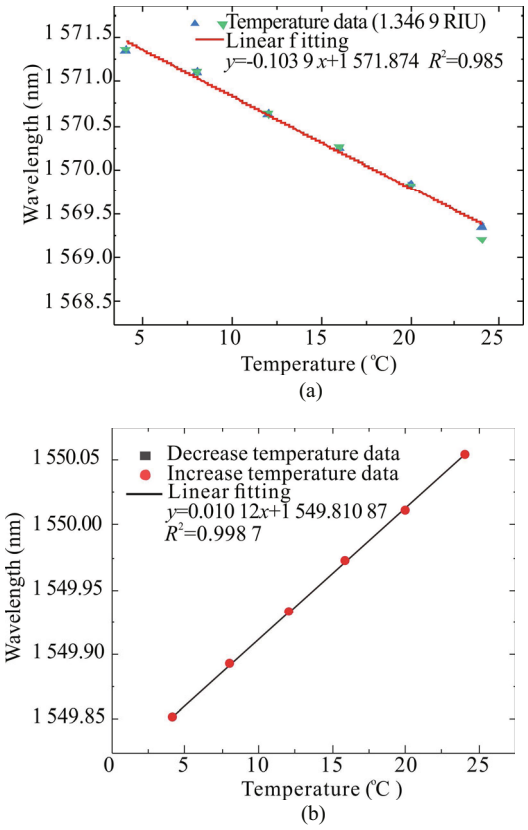


**Fig.7 (a) Fitting linear diagram of FP temperature sensor; (b) Fitting linear diagram of FBG temperature sensor**

As can be concluded, the sensor temperature and refractive index detection sensing can be distinguished by the above equation, refractive index or temperature parameters according to the measurement acquirement.

The stability is a very important technical index of sensor. To further demonstrate the correctness of our design and packaging methods, the response of the sensor at a determined temperature and concentration was tested experimentally. The sensor was placed in a solution with a concentration of 6%, and then placed all packaged device in a temperature controller under a stable state of 20 ℃ for 100 min. As shown in Fig.8, the maximum wavelength fluctuations of FP and FBG during the whole process were 0.005 nm and 0.005 27 nm, respectively. The standard deviation of 10 groups of data shown as the standard deviation of FBG is 0.001 4 nm, and that of FP is 0.002 58 nm. It can be seen that the sensor has good stability.

Aiming at the requirement of refractive index measurement under slightly varying temperature, a mechanism of simultaneous measurement of temperature and refractive index is proposed. A compact fiber refractive index sensor has been designed considerately. Based on

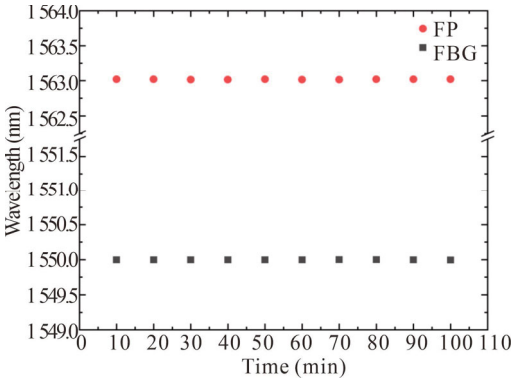


**Fig.8 Wavelength fluctuations of FBG and FP sensors with duration**

appropriate consideration, the proposed sensor has the following desirable features. The sensor allows simultaneous measurement of temperature and refractive index. The principle of refractive index and temperature sensing and the method of refractive index sensitization are theoretically simulated and analyzed. The refractive index sensitivity of the sensor is 1 108.413 5 nm/RIU, and the temperature sensitivities of FP and FBG are −0.103 9 nm/℃ and 0.010 1 nm/℃, respectively, and it has good linearity. The sensor has good stability. The sensor is small in size and simple in structure, and can be used in the field of biomedicine and battery electrolyte detection.

## Ethics declarations

## Conflicts of interest

The authors declare no conflict of interest.

## References

[1] LI X, LI F, ZHOU X, et al. Optic fiber DNA biosensor with temperature monitoring based on double microcavities Fabry-Perot interference and Vernier combined effect[J]. IEEE transactions on instrumentation and measurement, 2023, 1(72): 1-8.

[2] ZHAO Q, LIU J, YANG H, et al. Double U-groove temperature and refractive index photonic crystal fiber sensor based on surface plasmon resonance[J]. Applied optics, 2022, 61(24): 7225-7230.

[3] FEI Y, CUI T, MA C H, et al. Fiber optic sensors based on circular and elliptical polymer optical fiber for measuring refractive index of liquids[J]. Optical fiber technology, 2022, 68: 102812.

[4] QIAO S Y, CHEN X L, JIANG S, et al. Plasmonic fiber-optic sensing system for in situ monitoring the capacitance and temperature of supercapacitors[J]. Optics express, 2022, 30(15): 27322-27332.

[5] QIAN S, CHEN X, JIANG S, et al. Direct detection of charge and discharge process in supercapacitor by fiber-optic LSPR sensors[J]. Nanophotonics, 2020, 9(5): 1071-1079.

[6] SUN M, JIN Y, DONG X. All-fiber Mach-Zehnder interferometer for liquid level measurement[J]. IEEE sensors journal, 2015, 15(7): 3984-3988.

[7] WANG H, MENG H, XIONG R, et al. Simultaneous measurement of refractive index and temperature based on asymmetric structures modal interference[J]. Optics communications, 2016, 364: 191-194.

[8] HUANGAB J, HANC X, LIUD F, et al. Monitoring battery electrolyte chemistry via in-operando tilted fiber Bragg grating sensors[J]. Energy & environmental science, 2021, 14(12): 6464-6475.

[9] SUNTSOV S, RUTER C E, KIP D. Dual parameter fiber-integrated sensor for refractive index and temperature measurement based on Fabry-Perot micro-resonators[J]. Applied optics, 2019, 58(8): 2076-2080.

[10] ZHANG Y, XUE J, LIU W, et al. Measurement of liquid thermo-optical coefficient based on all-fiber hybrid FPI-SPR sensor[J]. Sensors & actuators A: physical, 2021, 331: 112954.

[11] WU C, LIU Z, ZHANG A P, et al. In-line open-cavity Fabry-Pérot interferometer formed by C-shaped fiber for temperature-insensitive refractive index sensing[J]. Optics express, 2014, 22(18): 21757-21766.

[12] LI F, LI X, ZHOU X, et al. Simultaneous measurement of temperature and relative humidity using cascaded C-shaped Fabry-Perot interferometers[J]. Lightwave technology, 2022, 40: 1209-1215.

[13] LI X, WARREN-SIMITH S C, XIE L, et al. Temperature-compensated refractive index measurement using a dual Fabry-Perot interferometer based on C-fiber cavity[J]. IEEE sensors journal, 2020, 20(12): 6408-6413.

[14] BAI Y L, YIN B. Simultaneous measurement of pressure and temperature based on processed capillary tube and fiber Bragg grating[J]. Optical engineering, 2016, 55(8): 080502.

[15] LIU Y, JING Z, LIU Q, et al. All-silica fiber-optic temperature-depth-salinity sensor based on cascaded EFPIs and FBG for deep sea exploration[J]. Optics express, 2021, 29: 23953-23966.

[16] TIAN M, LU P, CHEN L, et al. Femtosecond laser fabricated in-line micro multicavity fiber FP interferometers sensor (Article)[J]. Optics communications, 2014, 316: 80-85.

[17] LIU Y, LIANG X, LIU X, et al. A fiber temperature sensor based on micro-hole Fabry-Perot cavity[J]. Electro-optic technology application, 2018.

[18] XU F, LU L, LU W W, et al. In-line Fabry-Perot refractive index sensor based on microcavity[J]. Chinese optics letters, 2013, 11(8): 93-96.

[19] ZHU Z, BA D, LIU L, et al. Temperature-compensated multi-point refractive index sensing based on a cascaded Fabry-Perot cavity and FMCW interferometry[J]. Optics express, 2021, 29(12): 19034-19048.

[20] NI X, FU S, ZHAO Z. Thin-fiber-based Fabry-Pérot cavity for monitoring microfluidic refractive index[J]. IEEE photonics journal, 2016, 8(3): 1-7.

[21] ZHANG H, LIU C, HE L, et al. Joint-assisted open-cavity interferometer for high-precision temperature detection via strain crosstalk deduction and Vernier effect[J]. IEEE transactions on instrumentation and measurement, 2022, 71: 1-10.

[22] LIU Q, WANG C, LIU W, et al. Large-range and high-sensitivity fiber optic temperature sensor based on Fabry-Pérot interferometer combined with FBG[J]. Optical fiber technology, 2021, 68: 102794.

[23] CAO Y, LIU H, TONG Z, et al. Simultaneous measurement of temperature and refractive index based on a Mach-Zehnder interferometer cascaded with a fiber Bragg grating[J]. Optics communications, 2015, 342: 180-183.

[24] LAO J, SUN P, LIU F, et al. In situ plasmonic optical fiber detection of the state of charge of supercapacitors for renewable energy storage[J]. Light: science and applications, 2018, 7.